

# Effects of Soluble Ferri–Hydroxide Complexes on Microbial Neutralization of Acid Mine Drainage

A. AZRA BILGIN,\*  
JOANN SILVERSTEIN, AND  
MARK HERNANDEZ

Department of Civil, Environmental, and Architectural  
Engineering, University of Colorado, Boulder, Colorado 80309

Heterotrophic respiration of ferric iron by *Acidiphilium cryptum* was investigated in anoxic microcosms with initial media pH values from 1.5 to 3.5. No organic carbon consumption or iron reduction was observed with an initial pH of 1.5, indicating that *A. cryptum* may not be capable of iron respiration at this pH. Significant iron reduction was observed at pH 2.5 and 3.5, with different effects. When the initial pH was 3.5, pH increased to 4.7–5.5 over 60 days of incubation with simultaneous production of 0.4 g L<sup>-1</sup> Fe<sup>2+</sup>. However, at an initial pH of 2.5, no significant change in pH was observed during iron respiration, although the accumulation of soluble ferrous iron was significantly higher, averaging 1.1 g L<sup>-1</sup> Fe<sup>2+</sup>. The speciation of the ferric iron electron acceptor may explain these results. At pH values of 3.5 and higher, precipitated ferric hydroxide Fe(OH)<sub>3</sub> would have been the primary source of ferric iron, with reduction resulting in net production of OH<sup>-</sup> ions and the significant increases in media pH observed. However at pH 2.5, soluble complexes, FeOH<sup>2+</sup> and Fe(OH)<sub>2</sub><sup>+</sup>, may have been the more prevalent electron acceptors, and the alkalinity generated by reduction of complexed iron was low. The existence of charged ferri–hydroxide complexes at pH 2.5 was verified by voltammetry. Results suggest that initiation of bacterial iron reduction may result in neutralization of acid mine drainage. However, this effect is extremely sensitive to iron speciation within a relatively small and critical pH range.

## Introduction

Acid mine drainage (AMD) occurs when oxygen-laden water contacts rock surfaces containing pyrite (FeS<sub>2</sub>) minerals that have been exposed by mining and ore processing activity. The growth of autotrophic iron-oxidizing bacteria is essential to acid mine drainage formation under low pH conditions typical of weathered pyrite found in many hard-rock mining sites. Oxidation of pyrite by biologically produced ferric iron using O<sub>2</sub> is generally accepted as the major cause of AMD. At pH <4.5, AMD has devastating ecological consequences in pristine mountain watersheds (1, 2), and remediation efforts heretofore often are prohibitively expensive and can themselves cause significant disruption of the AMD sites.

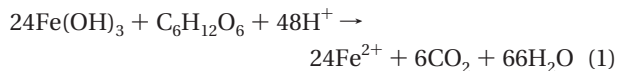
Numerous strains of heterotrophic acidophilic bacteria also have been identified in acid-generating rock formations (3). Researchers have suggested that enhancement of one heterotrophic metabolism, bacterial sulfate reduction, could

play a role in restoration of AMD sites (4, 5). However, typical AMD conditions often do not support bacterial sulfate reduction. Although SRB activity at relatively low pH has been reported, growth optima of many environmental isolates and sulfide production in microenvironments appear to be optimal above pH 5.5 (6, 7). In addition, it has been reported that the exothermic pyrite oxidation reaction generates sufficient heat to drive circulation of oxygen in unsaturated formations, making the transition from iron oxidation to sulfate reduction more difficult to obtain in AMD sources (8).

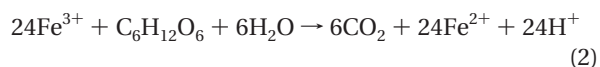
It is proposed that induction of bacterial iron reduction may be a more achievable mechanism for suppression of pyrite oxidation while generating alkalinity (5). Strains of facultative iron-reducing bacteria, adapted to acidic and aerobic or microaerophilic conditions, have been identified at AMD sites (9, 10). Iron oxidation produces copious amounts of oxidized iron Fe(III) species and ferric (oxy) hydroxide species, which could serve as electron acceptor species for iron respiration (5, 11). During iron respiration, ferric iron could be consumed by heterotrophic acidophilic bacteria, disrupting the pyrite oxidation cycle. In addition, lower redox conditions produced by iron reduction could create a more favorable environment for SRB growth. Finally, many iron respiring bacteria are facultative and would induce a transition from aerobic to anoxic respiration (12, 13). However, the lack of significant amounts of organic electron donors is probably the most significant limitation for heterotrophic growth in weathered rock formations. Marchand reported that growth of two *Acidiphilium* strains grown in cocultures with *Acidothiobacillus ferrooxidans* was significantly increased by addition of glucose (14). It has been suggested that addition of organic carbon to AMD-generating waste rock may induce iron reduction in situ with beneficial results for prevention or reversal of acid formation.

In addition to the consumption of ferric iron, bacterial iron respiration may result in other restorative effects. Various researchers have reported a pH increase during iron respiration reactions. Küsel et al. (10) compared the growth of *Acidiphilium cryptum* JF-5 on several carbon sources. Glucose was consumed under anoxic conditions without apparent delay and stimulated the formation of Fe(II) and CO<sub>2</sub>, and the pH increased from 3.2 to 5.8. When glucose was added to un-aerated cultures of *Acidiphilium acidophilus*, Marchand and Silverstein (14) observed a 2.5-unit pH increase during iron respiration. However, Bilgin and Silverstein (15) suggested that the initial pH at the onset of iron respiration may have a significant effect on pH change. They have observed similar rates of iron respiration (Fe<sup>2+</sup> production) by *A. cryptum*, with an initial pH of 2.2 and 1.8, but the final pH was markedly different, 4.8 and 1.8, respectively.

Speciation of the ferric iron electron acceptor may explain these findings (16). Stoichiometry for respiration of ferric hydroxide, using glucose and neglecting cell synthesis, predicts 2 mol of acidity consumed per mole of ferric iron reduced:



However, for the free ferric ion, 1 mol of acidity is produced per mole of iron reduced:



\* Corresponding author phone: 626-395-4406; fax: 626 395 2940; e-mail: abilgin@caltech.edu.

In addition to neutral ferric hydroxide and  $\text{Fe}^{3+}$  ion, Langmuir (17) reported that significant amounts of soluble iron hydroxide complexes are formed at pH greater than 2.2. Since typical AMD pH values are between 2 and 4 (18, 19), complexed iron species may be important in determining the feasibility of bacterial iron respiration as a means to mitigate acid mine drainage formation.

Marchand and Silverstein (14, 20) proposed that ferric iron speciation was important in the biogeochemical effects and the activity of heterotrophic bacteria in AMD; however, they were not able to confirm the existence of the different iron complexes using conventional analytical techniques or to verify their effect on iron respiration. For the research reported here, voltammetry was used to investigate ferric iron complex formation.

Voltammetry is an electrochemical method for analyzing solutions containing reducible and oxidizable charged species in real time. Electric potential (voltage) between two electrodes (indicator and reference) is varied in a regular manner while the current produced as a result of charged complex formation/consumption is monitored. The majority of chemical elements, and particularly metals, can be identified by reduction spectra recorded during voltammetric analysis. One method, Osteryoung square wave voltammetry (OSWV), has proved useful to investigate redox reactions (21), although there are no reports of its application to monitoring of iron-hydroxide complexation under environmental conditions. For this research, an OSWV method was developed to investigate the pH-associated changes in the charge and redox state of soluble iron species in both the free ion and hydroxide-complexed forms.

## Materials and Methods

The effect of initial pH on bacterial iron respiration and associated iron speciation and pH changes was investigated in flask cultures in the Environmental Engineering Laboratories at the University of Colorado, Boulder.

**Bacteria Cultures.** *A. cryptum* (ATCC 33463) was the heterotrophic iron reducing strain used in all experiments. Cultures were obtained from the American Type Culture Collection (ATCC, Manassas, VA) and maintained using glucose minimal media as described by Wichlaz and Unz (22).

**Microcosm Experiments.** Experiments were performed in 500-mL Erlenmeyer flasks mounted on a shaker table (New Brunswick Scientific Co. Inc., Edison, NJ) agitated at 200 rpm. The initial liquid volume of each microcosm was 300 mL, with 3 mL removed for each sample. Sterility was ensured by autoclaving the flasks at 121 °C and 15 psi for 15 min and sampling aseptically. At the beginning of the experiments, inoculated flasks were covered with cotton plugs to prevent contamination of the culture while allowing oxygen transfer into the flask. Experiments were started under aerobic conditions to determine the switch from aerobic to anoxic growth of the bacterial population. After a period of aerobic growth, flasks were capped with butyl rubber septa for anoxic growth. To all flasks was added 300 mL of LHET2 medium (23): 2 g of  $(\text{NH}_4)_2\text{SO}_4$ , 0.5 g of  $\text{K}_2\text{HPO}_4$ , 0.5 g of  $\text{MgSO}_4 \cdot 7\text{H}_2\text{O}$ , 0.1 g of KCl, 0.002 g of NaCl, 0.106 g of tryptic soy broth, and 0.1 g of yeast extract per liter of medium. Sampling continued as the headspace oxygen was consumed, and anoxic reactions occurred. Liquid samples were taken using a sterile 21-gauge needle and syringe. Ferric sulfate [ $\text{Fe}_2(\text{SO}_4)_3 \cdot 5\text{H}_2\text{O}$ ] (Fisher Scientific, Pittsburgh, PA) was added as the source of iron and added to obtain an initial ferric iron concentration of 1.2 g  $\text{L}^{-1}$  at 188 h. Glucose ( $\text{C}_6\text{H}_{12}\text{O}_6$ ) (Fisher Scientific) was the substrate for heterotrophic bacterial growth in all experiments, added to obtain an initial concentration of 5 g  $\text{L}^{-1}$  [2 g  $\text{L}^{-1}$  as total organic carbon (TOC)] at the beginning of the

experiments. Additional glucose, 2.5 g  $\text{L}^{-1}$  (1 g  $\text{L}^{-1}$  as TOC), was supplied to the flasks at 188 h.

*A. cryptum* growth experiments were conducted with varying initial pH values (1.5, 2.5, and 3.5), and duplicate flasks for each pH were maintained. Media pH was adjusted with HCl and NaOH just prior to inoculation. A control flask contained sterile growth media incubated under the same conditions as the growth flasks.

Efforts were made to ensure a uniform inoculum cell density in each flask. The DNA intercalating agent DAPI (4',6-diamidino-2-phenylindole) was used to quantify the cell density of *A. cryptum* in all the inoculated microcosms (24). Microscope counts of DAPI-stained samples indicated that the initial *A. cryptum* cell concentration in the flasks ranged from  $3.6 \times 10^6 \pm 0.7 \times 10^6$  to  $5.0 \times 10^6 \pm 1.6 \times 10^6$  cells/mL. Although DAPI stains both viable and nonviable intact cells, the flasks all were inoculated from log growth phase cultures.

**Iron.** Both soluble (filterable) and solid-phase (nonfilterable) iron were determined spectrophotometrically using 1,10-phenanthroline according to a modification of the procedure described in ref 25. Soluble ferrous iron chelates with 1,10-phenanthroline to form an orange complex that was measured at 510 nm in a spectrophotometer (Model UV160U, Shimadzu Corp., Kyoto, Japan). For the purpose of this study, "soluble" iron was defined as that fraction that passed through a 0.2  $\mu\text{m}$  filter. To measure the total filterable iron, all oxidized iron in the filtrate was reduced to the ferrous form using the chemical reducing agent hydroxylamine hydrochloride ( $\text{NH}_2\text{OH} \cdot \text{HCl}$ ) (Fisher Scientific) with total filterable iron concentration determined as above. The filterable ferric iron concentration was calculated by subtracting ferrous from total iron. The total iron in unfiltered samples was measured at the beginning and end of the experiments to determine the conservation of mass. The total iron was measured by digestion of unfiltered samples at 150 °C for 15 min in 25% hydroxylamine hydrochloride to convert both solid and soluble  $\text{Fe}^{3+}$  to  $\text{Fe}^{2+}$ , which was analyzed as described above.

**Total Organic Carbon, pH, and Dissolved Oxygen.** Total soluble organic carbon was used to monitor consumption of glucose during the experiments. The TOC of filtered samples was measured as the nonpurgable organic carbon fraction using an autoanalyzer (Model TOC 5000, Shimadzu Corporation, Kyoto, Japan). pH was monitored using a calomel electrode and pH meter (Accumet AB15 Basic & Biobasic, Fisher Scientific). Dissolved oxygen (DO) was measured using a probe (Model 5750 BOD Probe, YSI Incorporated, Yellow Springs, OH) and meter (Model 52 YSI Incorporated, Yellow Springs, OH).

**Fe(III)-Hydroxide Complexes.** For the ferric iron-hydroxide complexation experiments, voltammetric measurements were performed with a CV-50W voltammetric analyzer fitted with a controlled-growth mercury electrode; the multimode electrode was used in static mercury drop electrode (SMDE) mode. The mercury electrode was multiplexed using BAS commercial software (Bioanalytical Systems, Inc., Lafayette, IN), a platinum auxiliary electrode, and a Ag/AgCl (3 M KCl) reference electrode. All potentials were normalized to the Ag/AgCl electrode. A system scan rate of 5 mV  $\text{s}^{-1}$  was used with a drop time of 1 s. For OSWV, the pulse amplitude was 100 mV with a sample width of 17 ms. A repeatable drop size was produced using a borosilicate capillary tube. The time the solenoid was energized (valve open) was 100 ms for all runs. The supporting electrolyte was a solution of sodium carbonate (0.5 M) and oxalic acid (0.5 M) (26). A stock solution of ferric iron ( $3.6 \times 10^{-2}$  M) was prepared from  $\text{Fe}_2(\text{SO}_4)_3 \cdot 5\text{H}_2\text{O}$  that had been dehydrated by drying overnight at 100 °C. A stock solution of 1 N NaOH was prepared for OSWV generation of  $\text{Fe}(\text{OH})_n^{(3-n)+}$  complexes.

For each OSWV titration, 10 mL of electrolyte was added to the electrochemical cell.

In OSWV, a square wave potential is superimposed on a staircase potential between the anode and cathode in a solution containing charged species. The applied potential shifts toward the anode after each square wave cycle (21). In the case of reversible processes, the current peaks are Gaussian and the peak potentials are equal to the half potentials of the redox processes. The number of electrons involved in the redox reaction can be calculated from the half-peak widths, after accounting for the effects of temperature and the amplitude of the applied voltage (21). The Faradaic current is sampled at the end of each half cycle. Therefore, the current is sampled twice during each square wave: the top of each square waveform represents the reverse current, and the bottom, the forward current. The net current is the forward current minus the reverse current (21). Two sets of experiments were conducted. For the first set of experiments, 0.5 mL of Fe(III) stock solution was added to the cell, producing a sample concentration of  $1.8 \times 10^{-2}$  M. Titration continued with additions of 0.1 mL NaOH stock until all the iron had precipitated, as indicated by the disappearance of the current peak. A control titration was done using Milli-Q water as the titrant. The initial pH of the iron solution was 1.63, and the pH after precipitation of all ferric iron was 2.51. Corresponding current and potential values were recorded after each NaOH (or water) addition. For the second set of experiments, 0.05 mL of Fe(III) stock was added to the sample cell electrolyte (initial ferric iron concentration =  $1.8 \times 10^{-3}$  M) and titrated with NaOH starting with 0.5 mL, followed by additions of 0.02 mL NaOH until all the iron had precipitated. Initial pH was 1.67 and the titration was stopped at pH 2.34 before iron precipitation was complete. For the second titration, to calculate the stability constants of these complexes with the OSWV method, temperature was maintained at 30 °C with a thermostat-controlled electric heater. The overall stability constants ( $\beta$ ) of the  $\text{Fe}(\text{OH})_n^{(3-n)+}$  complexes were calculated using the DeFord–Hume Function (27).

## Results and Discussion

Figure 1a–e shows profiles for ferrous iron, dissolved oxygen, pH, ferric iron, and TOC, respectively, for the inoculated flasks with initial pH values of 1.5, 2.5, and 3.5. As shown in Figure 1a, accumulation of ferrous iron was observed in flasks inoculated with aerobically grown cultures of *A. cryptum* within 50 h after aeration ceased (at 188 h) in flasks with initial pH values of 2.5 and 3.5. No iron reduction occurred in sterile controls (data not shown), and no  $\text{Fe}^{2+}$  accumulated in the *A. cryptum* cultures inoculated at pH 1.5.

In addition, there were no changes in pH (Figure 1c), soluble ferric iron (Figure 1d), and TOC (Figure 1e) for the low pH cultures, suggesting that the experimental conditions tested were outside the tolerance range for *A. cryptum*. Dissolved oxygen profiles in Figure 1b are consistent with the ferrous iron trends: in flasks started at pH 2.5 and 3.5, dissolved oxygen decreased from 6 to less than approximately  $1 \text{ mg L}^{-1}$  within 50 h, consistent with the appearance of  $\text{Fe}^{2+}$ .

It is of interest that iron reduction began while dissolved oxygen was still present.  $\text{Fe}^{2+}$  was observed 24 h after aeration stopped in culture flasks at pH 2.5 and 3.5, although the dissolved oxygen at that time was over  $2 \text{ mg L}^{-1}$ . In fact, dissolved oxygen levels persisted near  $1 \text{ mg L}^{-1}$  throughout iron reduction, suggesting that *A. cryptum* cultures were capable of rapid transition from oxygen to iron as an electron acceptor. Similar observations have also been reported by Küsel et al. during microcosm studies conducted with coal mining lake sediments (28).

Consumption of organic carbon (Figure 1e) also followed the trends for appearance of ferrous iron in the pH 2.5 and

3.5 flasks, further supporting bacterial iron respiration as the cause of iron reduction. Significant differences in the extent of iron respiration and resulting changes in water chemistry were observed between the flasks started at pH 2.5 and 3.5, as discussed below.

An average of  $0.4 \text{ g L}^{-1}$  of soluble  $\text{Fe}^{2+}$  accumulated when the initial pH was 3.5, with over 90% of the accumulation within the first 450-h incubation. Ferrous iron accumulation represented only 33% of the ferric iron added. Reduction of added iron at pH 3.5 was significantly less than that for the flasks with initial pH of 2.5. The availability of soluble ferric iron, shown in Figure 1d, may provide an explanation for this difference. At the higher pH, soluble ferric iron was not detected after the first sample time, and the fact that only a fraction of added iron was reduced may have been the result of the ferric iron electron acceptor being in the solid phase. Other researchers have reported limitations on the extent of bacterial iron reduction when iron precipitates age and become more crystalline in structure (29–39). For the flask started at pH 3.5, the pH rose significantly during iron respiration, from 3.5 to over 5, also consistent with use of iron hydroxides as the electron acceptor in iron respiration. The fact that iron respiration appeared to stop altogether may have been due to formation of more crystalline and less bioavailable ferric iron, either due to aging or higher pH. To further investigate the iron mineral phase transformations that occur over the pH range of 3.5–5 in the media supplied, speciation calculations were conducted by using PhreeqC v.2 (40). Model results suggested that the predominant iron phases in the media at pH 3.5 are amorphous ferric hydroxides, goethite, hematite, and jarosite. It is known that goethite and hematite are the more crystalline structures of amorphous iron hydroxides and tend to form as amorphous ferric hydroxides age (17). Also confirmed with model results, as the environment become more reducing and the pH increases to 5, the dominant phases become goethite, hematite, and magnetite, indicating that the formation of less labile/crystalline iron oxides may be the cause of incomplete iron reduction. Bilgin et al. previously observed a plateau in Fe(II) production during iron respiration by *A. cryptum* at pH 5, and X-ray diffraction analysis conducted on the precipitates suggested that it may be due to formation and precipitation of Fe(II)–Fe(III) oxides (30).

Researchers have suggested that the presence of Fe(II) at elevated concentrations may have an effect on the bioavailability of iron (hydr)oxides (33, 34, 36–38). Roden et al. showed that the low microbial reducibility of crystalline Fe(III) oxides may be caused by sorption (adsorption and/or surface precipitation) of biogenic Fe(II) on oxide and Fe(III)-reducing bacterial surfaces (33, 34, 37, 38). Although their experiments were conducted at circumneutral pH and by neutrophilic, iron-reducing bacteria, sorption of Fe(II) onto iron (hydr)oxides produced during iron respiration may explain the slower reduction of iron (hydr)oxides observed in this paper. Fe(II) sorption may be a result of the lack of bioavailable iron (hydr)oxides, halting further Fe(III) reduction in flasks started at pH 3.5.

Iron respiration by anoxic *A. cryptum* cultures started at pH 2.5 resulted in  $1.1 \text{ g L}^{-1}$   $\text{Fe}^{2+}$  within the first 450 h of incubation (Figure 1a). Ferrous iron formation accounted for over 90% of ferric iron added to the medium at pH 2.5 and mirrored the decrease in soluble ferric iron species (Fe(III)), as shown in Figure 1d. Unlike the higher pH flasks, iron respiration by *A. cryptum* cultures grown at pH 2.5 did not result in a pH change in the media.

Figure 1e shows TOC consumption during both aerobic and anoxic growth of *A. cryptum* in the iron respiration experiments. Initial pH did not have a significant effect on TOC consumption during iron respiration; and the course of TOC consumption followed ferrous iron accumulation

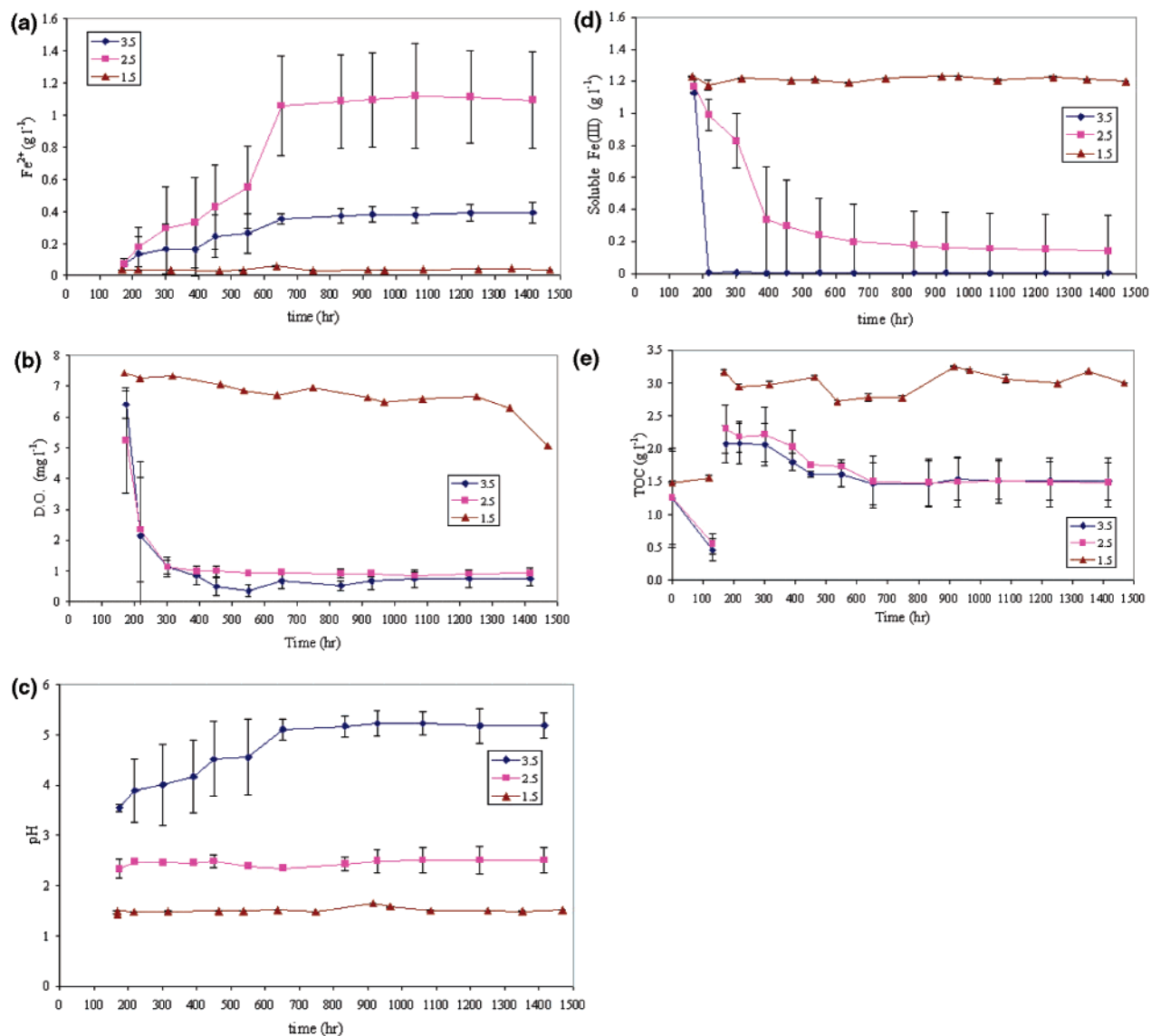


**FIGURE 1.** (a) Average soluble  $\text{Fe}^{2+}$  accumulation. (b) Dissolved oxygen (DO) profiles. (c) pH profiles. (d) Average soluble  $\text{Fe(III)}$  profiles. (e) Average TOC profiles in flask reactors with glucose and ferric iron media inoculated with *A. cryptum* with initial pH values of 1.5, 2.5, and 3.5. Ferric iron ( $\text{Fe}_2(\text{SO}_4)_3$ ) and glucose ( $2 \text{ g L}^{-1}$  as TOC) were added and aeration stopped after 188 h. Initial TOC is residual from aerobic incubation before aeration stopped. Data at pH 2.5 and 3.5 are averages of duplicate flasks in replicate experiments ( $n = 4$ ), and data are averages of duplicate flasks at pH 1.5 ( $n = 2$ ). Error bars for pH 2.5 and 3.5 are  $\pm 1$  standard deviation.

both at pH 3.5 and 2.5. The theoretical stoichiometry for the dissimilatory iron reduction in eqs 1 and 2 predicts that 18.6 g of  $\text{Fe}^{2+}$  would be produced per gram of TOC consumed, neglecting cell yield. It would therefore be expected that energy production from respiration yielding 0.4 and  $1.1 \text{ g L}^{-1}$  of  $\text{Fe}^{2+}$  would require on the order of 20–55  $\text{mg L}^{-1}$  of glucose TOC, respectively. However the amount of TOC consumed during the iron respiration experiments was significantly higher than that amount: approximately  $0.8 \text{ g L}^{-1}$  TOC was consumed at pH 2.5 by reduction of  $1.1 \text{ g L}^{-1}$  ferric iron, and  $0.6 \text{ g L}^{-1}$  TOC was consumed when iron respiration began at pH 3.5 during the reduction of  $0.4 \text{ g L}^{-1}$  iron. Residual oxygen in the headspace and trace amounts that persisted in the media (Figure 1b) could have supported glucose utilization in aerobic respiration, and cell synthesis would probably account for significant additional glucose consumption. The data in Figure 1d show that approximately  $1.5 \text{ g L}^{-1}$  TOC remained in the flask media for both pH values after 1200 h of incubation. The end of consumption of soluble TOC coincides with the plateau in production of  $\text{Fe}^{2+}$ , further

indicating that heterotrophic dissimilatory iron respiration was the principal activity in the flasks after aeration stopped.

The average pH change during iron respiration beginning at pH 2.5 was negligible in replicated experiments (Figure 1c). This result differed significantly from the 1.5-pH unit change in the culture flasks, where iron respiration started at pH 3.5. The pH increase observed in the higher pH media was consistent with reduction of solid-phase ferric hydroxide and associated release of acid-neutralization capacity. The lack of pH change during iron respiration at pH 2.5 may be explained by ferric iron speciation, as reported by Nordstrom (41). He found that equilibria for iron complexation reactions during pyrite oxidation resulted in a “crossover” point at pH 2.39. At pH greater than 2.39, oxidation of ferrous iron resulted in a decrease in solution pH due to increased formation of hydroxide solids, while pH increased during iron oxidation at pH < 2.39 with more free  $\text{Fe}^{3+}$  ion produced. At a pH near 2.39, however, the solution was buffered by hydrolysis reactions of the  $\text{Fe(III)}$  products,  $\text{Fe(OH)}_2^+$  and  $\text{FeOH}^{2+}$ . Iron complexation may have played a similar role during ferric

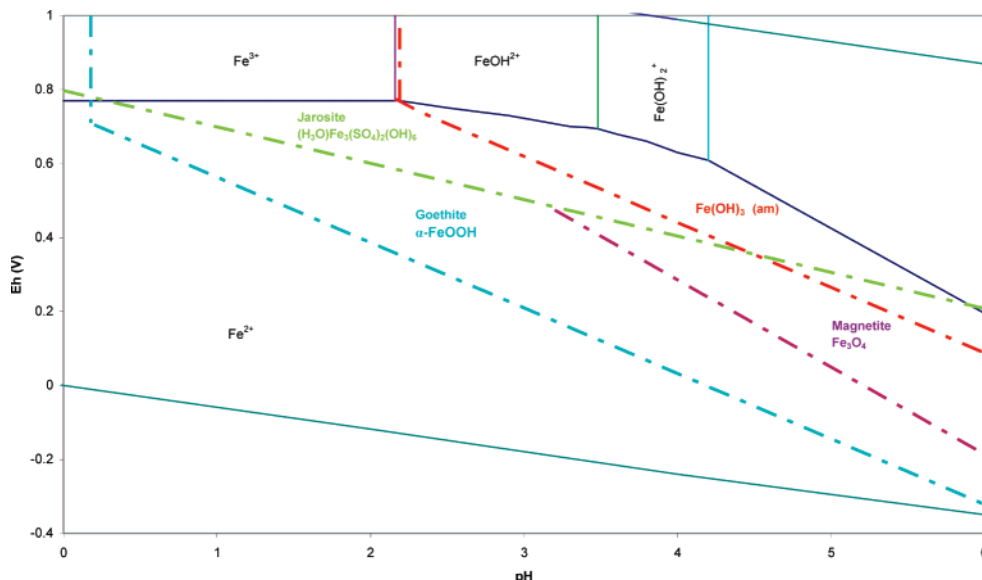
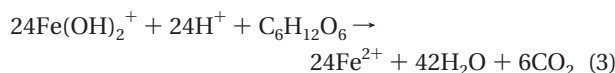


**FIGURE 2.** Eh–pH diagram for the Fe–O<sub>2</sub>–H<sub>2</sub>O system at 25 °C assuming  $pK_{sp} = 37.1$ ,  $pK_{sp} = 44.2$ ,  $pK_{sp} = 10.47$  for amorphous Fe(OH)<sub>3</sub>, goethite, and magnetite, respectively. Aqueous–solid boundaries are drawn for total dissolved iron concentrations of  $10^{-1.67}$  mol/kg (---), and  $10^{-8}$  mol/kg (—). Jarosite is also included in the system containing  $10^{-1.67}$  mol/kg of total dissolved iron assuming  $pK_{sp} = 5.39$ . Boundary equations are from Langmuir (17).

iron reduction by *A. cryptum*, in the reverse direction. At pH greater than the theoretical crossover point (3.5), the pH increase is due to consumption of Fe(OH)<sub>3</sub>(s). When Fe(III) respiration occurs at a pH near the ferric iron “crossover” point, pH changes could depend on the complexes present. Reduction of the dibasic ferric hydroxide complex would consume 1 mol of acidity per mole of complexed iron reduced:



However, use of ferric iron in the monobasic complex as the electron acceptor would produce no change in acidity:



Negligible pH changes observed when iron respiration started at pH 2.5 were consistent with utilization of the monobasic ferric hydroxide complex as the dominant electron acceptor (eq 4). Figure 2 is an Eh–pH diagram for the iron–oxygen–water system (also including jarosite) showing the effect of pH on iron speciation, using the equilibrium relations reported by Langmuir (17). According to the Eh–pH diagram (Figure 2) specific to the concentrations used in this experiment ( $10^{-1.67}$  mol/kg of total dissolved iron), under the initial aerobic conditions, the dominant iron phase in the system will be amorphous ferric hydroxides. The exact pH of the “crossover point” will depend on total iron concentration, as well as temperature. As total iron concentration increases, the pH for stability of Fe(OH)<sub>3</sub>(s) decreases. In the experiments reported here, the maximum soluble iron concentration was  $1.2 \text{ g L}^{-1}$  ( $10^{-1.67}$  M) just after the addition of Fe<sub>2</sub>(SO<sub>4</sub>)<sub>3</sub> to the microcosms (Figure 1d). According to Figure 2, at this concentration of ferric iron and under aerobic conditions as the initial conditions of experiments, at pH 3.5 the dominant Fe(III) species would be expected to be Fe(OH)<sub>3</sub>(s). However, at flask pH of 2.5, the formation of cationic ferric–hydroxy complexes may have buffered the media pH.

To confirm Fe(III) complexation near pH 2.5, two sets of voltammetric experiments were conducted. During the first set, NaOH was added to an 18 mM ferric iron solution, with an initial pH of 1.63, until no Fe(III) remained in the solution.

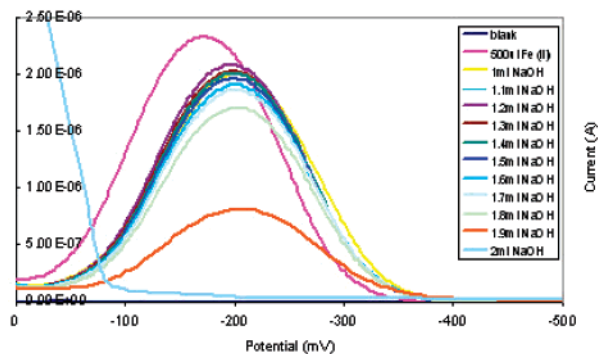


**FIGURE 3.** Current–voltage profiles during OSWV titration of ferric iron solutions (18 mM) with initial pH = 1.63: NaOH titrant, showing the formation of Fe(OH)<sub>n</sub><sup>(3–n)+</sup> with the associated shift of the current peak to the right (lower redox potential); decreasing the current peak indicates precipitation of ferric iron as Fe(OH)<sub>3</sub> with all ferric iron precipitated when the sample cell pH reached 2.51. (Complete precipitation shown in current profile line uniformly decreasing with no peak). Temperature for all titrations was not controlled and varied between 25 and 30 °C.

A significant and consistent shift in electrical potential was observed after the first NaOH addition, indicating that a charged ferric iron complex had been formed. The final pH after precipitation of all the iron was 2.51 (Figure 3). A control experiment with the 18 mM ferric iron solution titrated with water was conducted, and no electrical potential shift or pH change was observed.

To be able to identify any complexes formed during hydroxide titrations, a new voltammetry experiment was conducted with the temperature maintained at 30 °C so that the overall stability constants of the complexes could be calculated. The temperature increase to 30 °C was necessary because of the solubility of the electrolyte used in the analyses. As previously described, acidic (pH 1.67) ferric solutions (18 mM) were titrated with 1 N NaOH until a shift in the electrical potential peak was observed, indicating that a charged ferric iron complex had been formed. Figure 4 shows the current–potential diagram for one of the three replicate titrations. The overall stability constant for complex *i*, β<sub>*i*</sub>, is defined as

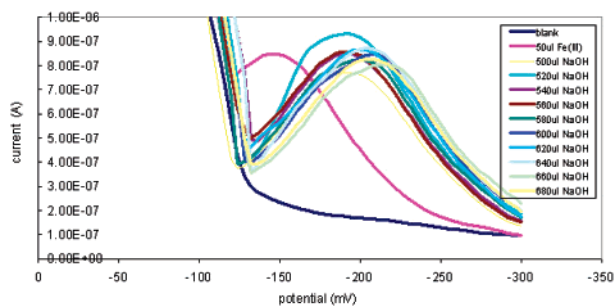
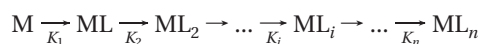


**FIGURE 4.** Current–voltage profiles during OSWV titration of ferric iron solutions (1.8 mM) with 1 N NaOH. Temperature was maintained at 30 °C throughout titration, and initial sample pH was 1.67. Formation of  $\text{Fe}(\text{OH})_n^{(3-n)+}$  is indicated by shift of the current peak to the right (lower redox potential); decreasing current peak height indicates precipitation of a fraction of initial ferric iron as  $\text{Fe}(\text{OH})_3$ . Titration ended when the sample cell pH reached 2.34 before all the iron had precipitated.

the equilibrium constant for the reaction in which the metal ion combines with the ligands necessary to form it (42).



In general,

$$\beta_i = \frac{[\text{ML}_i]}{[\text{M}][\text{L}]^i}$$

For the monobasic iron hydroxide complex,

$$\beta_1 = \frac{[\text{FeOH}^{2+}]}{[\text{Fe}^{3+}][\text{OH}^-]}$$

and for the dibasic ferric hydroxide complex,

$$\beta_2 = \frac{[\text{Fe}(\text{OH})_2^+]}{[\text{Fe}][\text{OH}^-]^2}$$

The overall stability constants of the complexes were calculated according to the method developed by DeFord and Hume (27). Under the experimental conditions at the initiation of iron respiration by *A. cryptum*, calculations using the DeFord–Hume function indicated that two ferric hydroxide complexes were present at pH 2.34:  $\text{FeOH}^{2+}$  and  $\text{Fe}(\text{OH})_2^+$ . The stability constants calculated from the voltammetry measurements were  $\log(\beta_1) = -3.02$  and  $\log(\beta_2) = -5.57$ , respectively, which fall within the range of values observed by previous researchers at 25 °C using other methods:  $-2.19$  and  $-5.67$  (43) and  $-3.05$  and  $-6.31$  (44), for  $\text{FeOH}^{2+}$  and  $\text{Fe}(\text{OH})_2^+$ , respectively.

#### Impact of Iron Respiration on Acid Mine Drainage.

Results of the iron respiration experiments indicate that geochemical conditions, particularly pH and resulting iron speciation, would have a significant effect on the role of bacterial iron respiration in remediation of acid mine drainage with a typical pH range of 2 to 4. At pH values where the electron acceptor would have been primarily uncharged ferric hydroxide, bacterial iron respiration resulted in increased pH, as well as reduced availability of ferric iron oxidant for pyrite oxidation. In addition, higher pH conditions would favor precipitation of other contaminant metal ions and growth of sulfate reducing bacteria. At somewhat lower pH values, where complexed ferric iron species would be the prevalent form of electron acceptor, iron reduction appears to proceed until the electron donor is completely consumed. Although not producing a pH increase, iron respiration is still an important mechanism, since exhaustion of ferric iron

oxidant would halt future pyrite oxidation. The results of this research indicate that iron respiration is a factor in initiating a transition from aerobic pyrite oxidation, and the availability of organic substrate is the key factor in this process, to induce oxygen depletion and provide electrons for iron respiration. The results show that the effect of carbon addition is more complex than what was initially anticipated, although the overall effect whenever iron respiration occurred was the elimination of ferric iron oxidant from the AMD generation cycle. Future research on acidophilic iron respiration by native mixed populations and on the long-term effects of carbon addition will be critical in developing a microbial process for in situ inhibition of acid drainage formation.

#### Acknowledgments

We would like to thank Dr. Kirk Nordstrom for his review of iron speciation results and Dr. Muna Abu-Dalo for her key contributions to the voltammetry experiments. We would also like to thank our three anonymous reviewers for their valuable comments, which made our discussions stronger.

#### Literature Cited

- (1) Tate, C. M.; Broshears, R. E.; McKnight, D. M. Phosphate dynamics in an acidic mountain stream—Interactions involving algal uptake, sorption by iron-oxide, and photoreduction. *Limnol. Oceanogr.* **1995**, *40* (5), 938–946.
- (2) Niyogi, D. K.; McKnight, D. M.; Lewis, W. M. Influences of water and substrate quality for periphyton in a montane stream affected by acid mine drainage. *Limnol. Oceanogr.* **1999**, *44*, 804–809.
- (3) Pronk, J. T.; Johnson, D. B. Oxidation and reduction of iron by acidophilic bacteria. *Geomicrobiol. J.* **1992**, *10*, 153–171.
- (4) Ferris, F. G.; Schultze, S.; Witten, T. C.; Pyfe, W. S.; Beveridge, T. J. Metal interactions with microbial biofilms in acidic and neutral pH environments. *Appl. Environ. Microbiol.* **1989**, *55* (5), 1249–1257.
- (5) Küsel, K.; Dorsch, T. Effect of supplemental electron donors on the microbial reduction of Fe(III), sulfate, and  $\text{CO}_2$  in coal mining-impacted freshwater lake sediments. *Microbial Ecol.* **2000**, *40*, 238–249.
- (6) Fortin, D.; Davis, B.; Southam, G.; Beveridge, T. J. Biogeochemical phenomena induced by bacteria within sulfidic mine tailings. *J. Ind. Microbiol.* **1995**, *14*, 178–185.
- (7) Wielinga, B.; Lucy, J. K.; Moore, J. N.; Seastone, O. F.; Gannon, J. E. Microbiological and geochemical characterization of fluvially deposited sulfidic mine tailings. *Appl. Environ. Microbiol.* **1999**, *65* (4), 1548–1555.
- (8) Lefebvre, R.; Hockley, D.; Smolensky, J.; Gelinat, P. Multiphase transfer processes in waste rock piles producing acid mine drainage 1: Conceptual model and system characterization. *J. Contam. Hydrol.* **2001**, *52* (1–4), 137–164.
- (9) Colberg, P. J. S. Role of sulfate in microbial transformations of environmental contaminants: Chlorinated aromatic compounds. *Geomicrobiol. J.* **1990**, *8*, 147–165.
- (10) Küsel, K.; Dorsch, T.; Acker, G.; Stackerbrandt, E. Microbial reduction of Fe(III) in acidic sediments: Isolation of acidiphilium cryptum JF-5 capable of coupling the reduction of Fe(III) to the oxidation of glucose. *Appl. Environ. Microbiol.* **1999**, *65* (8), 3633–3640.
- (11) Ribet, I.; Ptacek, C. J.; Blowes, D. W.; Jambor, J. L. The potential for metal release by reductive dissolution of weathered mine tailings. *J. Contam. Hydrol.* **1995**, *17*, 239–273.
- (12) Chapelle, F. H. *Groundwater Microbiology and Geochemistry*; John Wiley and Sons: New York, 1992; p 424.
- (13) Meier, J.; Babenzien, H.-D.; Wendt-Potthoff, K. Microbial cycling of iron and sulfur in sediments of acidic and pH-neutral mining lakes in Lusatia (Brandenburg, Germany). *Biogeochemistry* **2004**, *67*, 135–156.
- (14) Marchand, E. A.; Silverstein, J. The role of enhanced heterotrophic bacterial growth on iron oxidation by *Acidithiobacillus ferrooxidans*. *Geomicrobiol. J.* **2003**, *20*, 231–244.
- (15) Bilgin, A. A.; Silverstein, J. In *Role of Bacterial Iron Respiration in in-situ Restoration of Acid Mine Drainage*; 7th International Conference on Environmental Issues and Waste Management in Energy and Mineral Production, Cagliari, Italy, 2002; Ciccu, R., Ed.; SWEMP c/o DIGITA: Cagliari, Italy, 2002; pp 737–744.

- (16) Pronk, J. T.; Liem, K.; Bos, P.; Kuenen, J. G. Energy transduction by anaerobic ferric iron respiration in *Thiobacillus ferrooxidans*. *Appl. Environ. Microbiol.* **1991**, *57* (7), 2063–2068.
- (17) Langmuir, D. *Aqueous Environmental Geochemistry*; Prentice Hall: New York, 1997.
- (18) Nordstrom, K. D. Chemical modeling of acid mine waters in the Western United States. US Geological Survey Water Research Investment Report No. 91–4034, 534–538, 1991.
- (19) Plumlee, G. S.; Smith, K. S.; Montour, M. R.; Ficklin, W. S.; Mosier, E. Geologic controls on the composition of natural waters and mine waters draining diverse mineral-deposit types. In *The Environmental Geochemistry of Mineral Deposits. Part B. Case Studies and Research Topics*; Filipek, L. H., Plumlee, G. S., Eds.; Society of Economic Geologists (SEG): Littleton, CO, 1999; pp 373–432.
- (20) Marchand, E. A.; Silverstein, J. Influence of heterotrophic microbial growth on biological oxidation of pyrite. *Environ. Sci. Technol.* **2002**, *36*, 5483–5490.
- (21) Barker, G.; Jenkins, I. Square-wave polarography. *Analyst* **1952**, *77* (685), 685–696.
- (22) Wichlacz, P. L.; Unz, R. F. Acidophilic, heterotrophic bacteria of acidic mine waters. *Appl. Environ. Microbiol.* **1981**, *41* (5), 1254–1261.
- (23) Atlas, R. M. *Handbook of Microbiological Media*; CRC Press: Boca Raton, FL, 1997; p 760.
- (24) Porter, K. G.; Feig, Y. S. The use of DAPI for identifying and counting aquatic microflora. *Limnol. Oceanogr.* **1980**, *25* (5), 943–948.
- (25) APHA, AWWA, WEF. *Standard Methods for the Examination of Water and Wastewater*; American Public Health Association: Washington, DC, 1998.
- (26) Tackett, S.; Wieserma, L. Simultaneous polarographic determination of iron(II) and iron(III) in coal mine wastewater. *Anal. Lett.* **1972**, *5* (9), 643–648.
- (27) DeFord, D.; Hume, D. The determination of consecutive formation constants of complex ions from polarographic data. *J. Am. Chem. Soc.* **1951**, *73*, 5321–5322.
- (28) Küsel, K.; Roth, U.; Drake, H. L. Microbial reduction of Fe(III) in the presence of oxygen under low pH conditions. *Environ. Microbiol.* **2002**, *4* (7), 414–421.
- (29) Liu, C.; Kota, S.; Zachara, J. M.; Fredrickson, J. K.; Brinkman, C. K. Kinetic analysis of the bacterial reduction of goethite. *Environ. Sci. Technol.* **2001**, *35*, 2482–2490.
- (30) Bilgin, A. A.; Silverstein, J.; Jenkins, J. D. Iron respiration by *Acidiphilium cryptum* at pH 5. *FEMS Microbiol. Ecol.* **2004**, *49*, 137–143.
- (31) Roden, E. E. Fe(III) Oxide reactivity toward biological versus chemical reduction. *Environ. Sci. Technol.* **2003**, *37*, 1319–1324.
- (32) Roden, E. E.; Urrutia, M. M. Influence of biogenic Fe(II) on bacterial crystalline Fe(III) oxide reduction. *Geomicrobiol. J.* **2002**, *19*, 209–251.
- (33) Roden, E. E.; Urrutia, M. M.; Mann, C. J. Bacterial reductive dissolution of crystalline Fe(III) oxide in continuous-flow column reactors. *Appl. Environ. Microbiol.* **2000**, *66*, 1062–1065.
- (34) Roden, E. E.; Zachara, J. M. Microbial reduction of crystalline Fe(III) oxides: Role of oxide surface area and potential for cell growth. *Environ. Sci. Technol.* **1996**, *30*, 1618–1628.
- (35) Royer, R. A.; Burgos, W. D.; Fisher, A. F.; Jeon, B. H.; Unz, R. F.; Dempsey, B. A. Enhancement of hematite bioreduction by natural organic matter. *Environ. Sci. Technol.* **2002**, *36*, 1939–1946.
- (36) Royer, R. A.; Dempsey, B. A.; Jeon, B. H.; Burgos, W. D. Inhibition of biological reductive dissolution of hematite by ferrous iron. *Environ. Sci. Technol.* **2004**, *38*, 187–193.
- (37) Urrutia, M. M.; Roden, E. E.; Fredrickson, J. K.; Zachara, J. M. Microbial and surface chemistry controls on reduction of synthetic Fe(III) oxide minerals by the dissimilatory iron-reducing bacterium *Shewanella alga*. *Geomicrobiol. J.* **1998**, *15* (4), 269–291.
- (38) Urrutia, M. M.; Roden, E. E.; Zachara, J. M. Influence of aqueous and solid-phase Fe(II) complexants on microbial reduction of crystalline iron(III) oxides. *Environ. Sci. Technol.* **1999**, *33*, 4022–4028.
- (39) Nordstrom, K. D. Advances in the hydrogeochemistry and microbiology of acid mine waters. *Int. Geol. Rev.* **2000**, *42*, 449–515.
- (40) Parkhurst, D. L.; Appelo, C. A. J. *User's Guide to PhreeqC (version 2)—A computer program for speciation, batch-reaction, one-dimensional transport, and inverse geochemical calculations*; 99–4259; U.S. Geological Survey: Denver, CO, 1999; p 312.
- (41) Nordstrom, K. D. Advances in the hydrogeochemistry and microbiology of acid mine waters. *Int. Geol. Rev.* **2000**, *42*, 449–515.
- (42) Snoeyink, V.; Jenkins, D. *Water Chemistry*; John Wiley & Sons: New York, 1980; p 463.
- (43) Benjamin, M. M. *Water Chemistry*. 1st ed.; McGraw-Hill: New York, 2002.
- (44) Stumm, W.; Morgan, J. J. *Aquatic Chemistry: An Introduction Emphasizing Chemical Equilibria in Natural Waters*; John Wiley: New York, 1981; p 780.

Received for review February 16, 2005. Revised manuscript received July 1, 2005. Accepted July 27, 2005.

ES050315K